JGR Atmospheres

RESEARCH ARTICLE
10.1029/2020JD033158

# Tropical Expansion Driven by Poleward Advancing Midlatitude Meridional Temperature Gradients

**Hu Yang[1], Gerrit Lohmann[1], Jian Lu[2], Evan J. Gowan[1], Xiaoxu Shi[1], Jiping Liu[3], and Qiang Wang[1]**

[1]Alfred Wegener Institute, Helmholtz Centre for Polar and Marine Research, Bremerhaven, Germany, [2]Atmospheric Sciences and Global Change Division, Pacific Northwest National Laboratory, Richland, WA, USA, [3]Department of Atmospheric and Environmental Sciences, University at Albany, State University of New York, Albany, NY, USA

**Key Points:**
- Evidence shows that the tropical width follows the displacement of midlatitude meridional temperature gradients (MMTG)
- Under global warming, the MMTG advance toward the poles due to enhanced subtropical ocean warming
- Poleward advance of the MMTG shifts the edges of the tropics and subtropical climate zone toward poles

**Correspondence to:**
H. Yang,
hyang@awi.de

**Citation:**
Yang, H., Lohmann, G., Lu, J., Gowan, E. J., Shi, X., Liu, J., & Wang, Q. (2020). Tropical expansion driven by poleward advancing midlatitude meridional temperature gradients. *Journal of Geophysical Research: Atmospheres*, *125*, e2020JD033158. https://doi.org/10.1029/2020JD033158

Received 24 MAY 2020
Accepted 12 JUL 2020
Accepted article online 29 JUL 2020

**Abstract** An abundance of evidence indicates that the tropics are expanding. Despite many attempts to decipher the cause, the underlying dynamical mechanism driving tropical expansion is still not entirely clear. Here, based on observations, multimodel simulations from the Coupled Model Intercomparison Project phase 5 (CMIP5) and purposefully designed numerical experiments, the variations and trends of the tropical width are explored from a regional perspective. We find that the width of the tropics closely follows the displacement of oceanic midlatitude meridional temperature gradients (MMTG). Under global warming, as a first-order response, the subtropical ocean experiences more surface warming because of the mean Ekman convergence of anomalously warm water. The enhanced subtropical warming, which is partially independent of natural climate oscillations, such as the Pacific Decadal Oscillation, leads to poleward advance of the MMTG and drives the tropical expansion. Our results, supported by both observations and model simulations, imply that global warming may have already significantly contributed to the ongoing tropical expansion, especially over the ocean-dominant Southern Hemisphere.

**Plain Language Summary** Both observations and climate simulations have shown that the edges of tropics and associated subtropical climate zone are shifting toward higher latitudes under climate change. The underlying dynamical mechanism driving this phenomenon that has puzzled the scientific community for more than a decade, however, is still not entirely clear. A number of investigations argued that the atmospheric processes, in the absence of the ocean dynamics, lead to the tropical expansion. For example, increasing greenhouse gases, decreasing ozone and increasing aerosols are suggested to be the dominant factors contributing to expanding the tropics. However, these investigations are mostly based on model simulations, and observations show a much more complex evolution of expanding tropics. By examining the tropical width individually over each ocean basin, in this study, we find that the width of the tropics closely follows the displacement of oceanic midlatitude meridional temperature gradients (MMTG). Under global warming, as a first-order response, the subtropical convergence zone experiences more surface warming due to background convergence of surface water. Such warming induces poleward shift of the oceanic MMTG and drives the tropical expansion.

## 1. Introduction

The tropics are the warmest regions of the globe, where the Hadley circulation exists. The center of the tropics is characterized by rising air and vigorous convection, known as the Intertropical Convergence Zone (ITCZ), while the boundaries of the tropics are delineated by descending air and dry climate. Variations of the tropical width shape the patterns of precipitation, heat waves, storm tracks, and ocean circulation and therefore have broad social and environmental implications (Heffernan, 2016).

During the past 15 years, abundant evidence indicates that the boundaries of the tropics and the associated subtropical climate zone are shifting toward higher latitudes under climate change, a shift commonly referred to as tropical expansion (Archer & Caldeira, 2008; Bender et al., 2012; Cai & Cowan, 2013; Fu et al., 2006; Hu & Fu, 2007, 2018; Hu et al., 2013; Johanson & Fu, 2009; Lu et al., 2007; Norris et al., 2016; Seidel et al., 2008). This has been manifested in the poleward shift of the storm tracks (Yin, 2005), westerlies (Chen et al., 2008), jet streams (Archer & Caldeira, 2008), precipitation patterns (Scheff & Frierson, 2012), and clouds (Norris et al., 2016).

**Table 1**
*List of CMIP5 Models Used in This Study*

| Model name | Institutions |
|---|---|
| ACCESS1.0. | Centre for Australian Weather and Climate Research |
| ACCESS1.3. | Centre for Australian Weather and Climate Research |
| CanESM2 | Canadian Centre for Climate Modelling and Analysis |
| CNRM-CM5 | Centre National de Recherches Meteorologiques / Europeen de Recherche et Formation Avancees en Calcul Scientifique |
| CNRM-CM5.2 | Centre National de Recherches Meteorologiques / Centre Europeen de Recherche et Formation Avancees en Calcul Scientifique |
| CSIRO-Mk3.6.0 | Commonwealth Scientific and Industrial Research Organisation in collaboration with the Queensland Climate Change Centre of Excellence |
| GFDL-CM3 | Geophysical Fluid Dynamics Laboratory |
| GFDL-ESM2G | Geophysical Fluid Dynamics Laboratory |
| GFDL-ESM2 M | Geophysical Fluid Dynamics Laboratory |
| GISS-E2-H | NASA Goddard Institute for Space Studies |
| GISS-E2-R | NASA Goddard Institute for Space Studies |
| HadGEM2-ES | Met Office Hadley Centre and Instituto Nacional de Pesquisas Espaciais |
| INM-CM4 | Institute for Numerical Mathematics |
| IPSL-CM5A-LR | Institut Pierre-Simon Laplace |
| IPSL-CM5A-MR | Institut Pierre-Simon Laplace |
| IPSL-CM5B-LR | Institut Pierre-Simon Laplace |
| MIROC-ESM. | Japan Agency for Marine Earth Science and Technology, Atmosphere and Ocean Research Institute (The University of Tokyo), and National Institute for Environmental Studies |
| MIROC5 | Atmosphere and Ocean Research Institute (The University of Tokyo), National Institute for Environmental Studies, and Japan Agency for Marine-Earth Science and Technology |
| MPI-ESM-LR | Max Planck Institute for Meteorology (MPI-M) |
| MPI-ESM-MR | Max Planck Institute for Meteorology (MPI-M) |
| MPI-ESM-P | Max Planck Institute for Meteorology (MPI-M) |
| MRI-CGCM3 | Meteorological Research Institute |
| NorESM1-M | Norwegian Climate Centre |
| NorESM1-ME | Norwegian Climate Centre |

Despite many investigations to disentangle the cause, the underlying dynamical mechanism driving tropical expansion is still not entirely clear (Shaw, 2019; Staten et al., 2018). A number of investigations suggest that atmospheric processes, in the absence of the ocean dynamics, lead to tropical expansion. For example, model simulations suggest that increasing greenhouse gases (GHG) (Lu et al., 2007), stratospheric ozone depletion (Polvani et al., 2011; Thompson et al., 2011), and increasing aerosols (Allen et al., 2012) are the dominant contributors to expand the tropics. However, compared to model simulations, observations show a much more complex evolution of expanding tropics in respect to its magnitude, regional characteristic, and inter-annual variations (Allen & Kovilakam, 2017; Grise et al., 2019; Staten et al., 2018).

Proxies of past climate reveal that the subtropical climate zone also migrated in past glacial-interglacial cycles (Bard & Rickaby, 2009; Benz et al., 2016; Gersonde et al., 2005; Toggweiler & Russell, 2008). But, so far, there is no evidence of glacial-interglacial variability in ozone or aerosols. Concentration of GHG varied considerably over glacial-interglacial cycles (Petit et al., 1999). However, atmospheric sensitivity simulations (Grise & Polvani, 2014) illustrate that the direct radiative effect of GHG has very limited contribution to expanding the tropics (Staten et al., 2012). Recent studies (Yang et al., 2016, 2020) indicate that the large-scale ocean circulation is also shifting toward higher latitudes, raising the question of whether the ocean is driving the changes in atmospheric circulation. Indeed, studies have found that spatial variations in sea surface temperature (SST), in particular, the cold phase of Pacific Decadal Oscillation (PDO, Mantua et al., 1997), are related to the observed tropical expansion. Hence, a growing body of literature supports the idea that the observed expanding tropics are due to natural climate oscillations (Allen & Kovilakam, 2017; Allen et al., 2014; Grassi et al., 2012; Grise et al., 2018, 2019; Lucas & Nguyen, 2015; Mantsis et al., 2017; Nguyen et al., 2013; Tandon & Cane, 2017).

Most of the previous research examines the width of the tropics in a zonal mean framework, in which the regional characteristics of the tropical belt is masked by the zonal average. In this study, we explore the mechanism driving the tropical expansion by examining the variability and trend of the tropical width

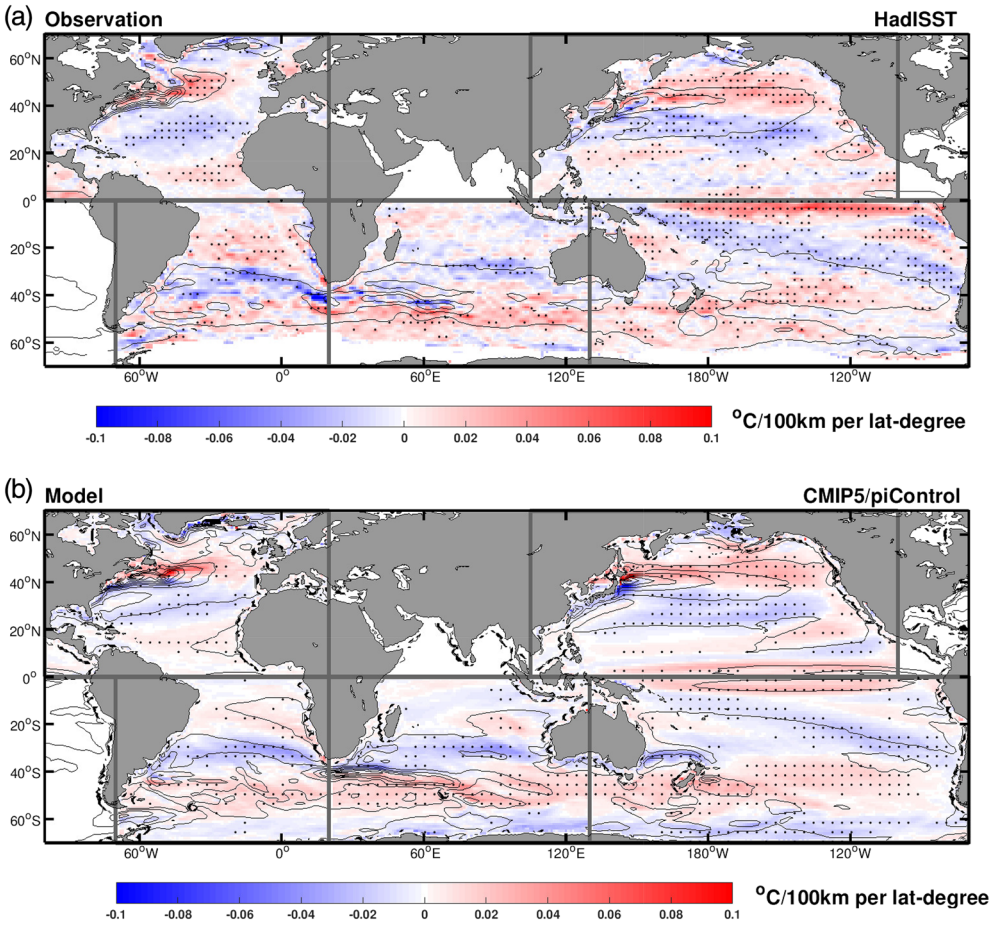


**Figure 1.** Patterns of meridional SST gradient anomalies associated with wider tropics. Results are conducted by regressing the annual mean width of tropics against the annual mean absolute value of meridional SST gradients (shading). Contours show the climatology meridional SST gradients. (a) Observational results based on ERA5 and HadISST data sets. Stippling indicates regions where the regression passes the 95% confidence level (Student's *t* test). (b) Multimodel ensemble mean result based on piControl experiment from CMIP5. Stippling indicates regions where more than 75% of the models agree on the sign of the regression values. Note that the regressions are performed for each ocean basin separately.

individually over each ocean basin. We find that the tropical width closely follows the meridional variations of the oceanic midlatitude meridional temperature gradient (MMTG). In a warming climate, an enhanced ocean surface warming in the subtropical convergence zone (SCZ) causes a poleward advance of the MMTG, which drives the tropical expansion and shifts the westerly winds, jet streams, and storm tracks toward higher latitudes.

## 2. Materials and Methods

### 2.1. Data and Method

The width of tropics in each ocean basin is defined by a common metric of the latitude where the near-surface zonal wind changes from easterly to westerly within the 20–40° latitude bands (USF). The USF metric is selected because it is representative of the tropical width and shows significant positive correlation with many of the other metrics, such as the metrics based on the meridional streamfunction, eddy-driven jet, precipitation minus evaporation, and the subtropical high (Waugh et al., 2018). Here, we use the near-surface wind based on the state-of-the-art high resolution (0.25° × 0.25°) atmospheric reanalysis ERA5 data set (Hersbach et al., 2019). Given that the original ERA5 data can only distinguish change in wind direction on a 0.25° resolution, we further linearly interpolate the zonal wind data to 0.01° resolution, in order to avoid the resolution-induced jumps in the evolution of tropical width.

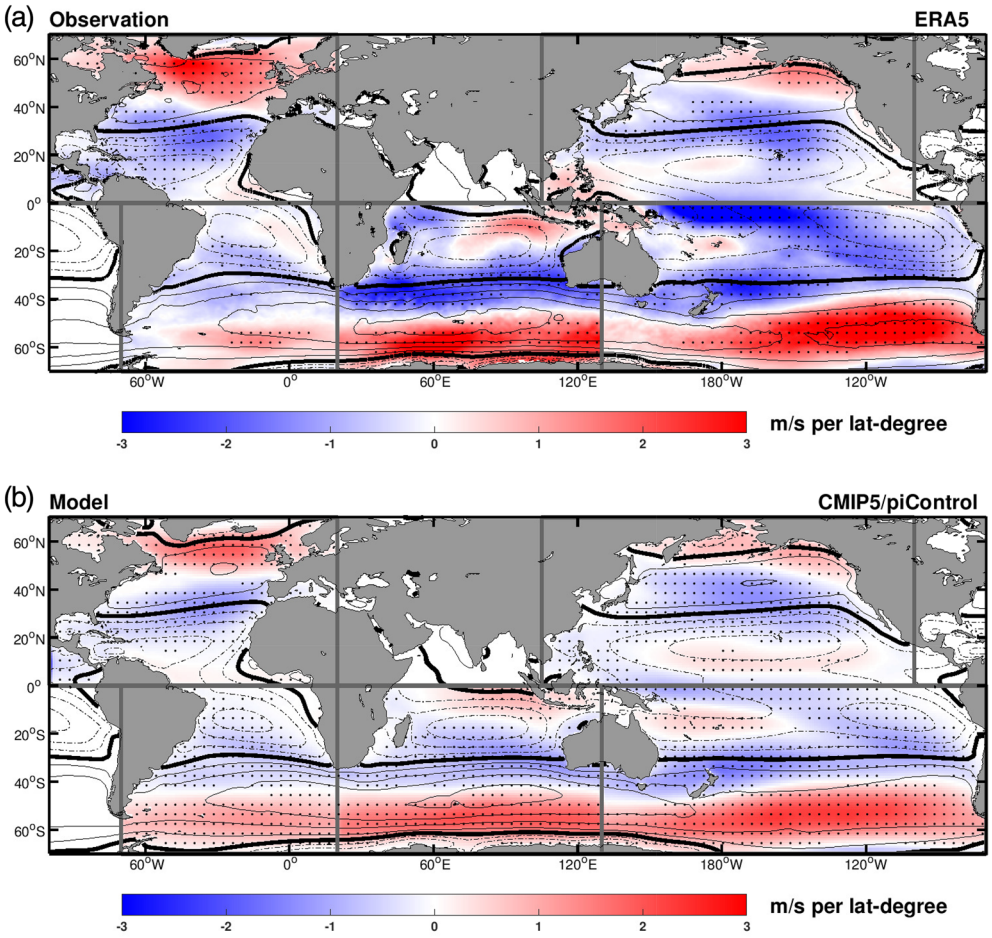


**Figure 2.** Patterns of zonal near-surface wind anomaly associated with poleward displacement of oceanic MMTG. Shading shows the regression of indices of meridional variations of MMTG against the zonal near-surface wind. Contours give the climatology zonal near-surface wind. Easterly winds are in dashed lines; westerly winds are in solid lines; zero zonal winds are bold. (a) Observational results. Stippling indicates regions where the regression passes the 95% confidence level (Student's *t* test). (b) Multimodel ensemble result based on CMIP5. Stippling indicates regions where more than 75% of the models agree on the sign of the regression values.

We compare the variations of the tropical width with that of the meridional variations of MMTG. The latter is defined as the weighted latitudinal position of meridional SST gradients at each ocean basin between 25° and 55°, following the equation below:

$$Y_{MMTG} = \left(\int_{25^\circ}^{55^\circ} G_{sst}(y)\cdot y dy\right)\left(\int_{25^\circ}^{55^\circ} G_{sst}(y) dy\right) \quad (1)$$

where $Y_{MMTG}$ represents the meridional position of MMTG, $G_{sst}$ is the absolute value of meridional SST gradient, and $y$ is the latitude. The Hadley Centre Global Sea Ice and Sea Surface Temperature (HadISST) (Rayner et al., 2003) data set is used to compute the meridional variations of oceanic MMTG and the temporal SST trend. The satellite-based SST, that is, the Optimum Interpolation Sea Surface Temperature (OISST) data set, is also used to cross validate the SST trend derived from HadISST data set.

Since the satellite observational SST only covers four decades, the decadal natural variability, such as the PDO, may contribute to the linear trend. In our analysis, we also provide the SST trend without the PDO signal, in which the PDO signal is identified and removed from the original SST records by performing a linear regression of the SST variability with respect to the PDO index (Mantua et al., 1997). A similar approach has also been applied by Ionita et al. (2014). To understand the pattern of SST warming, the ocean reanalysis data set, Simple Ocean Data Assimilation (SODA2.2.0, 1948–2008, Carton & Giese, 2008), is also used to create the structure of background ocean circulation.

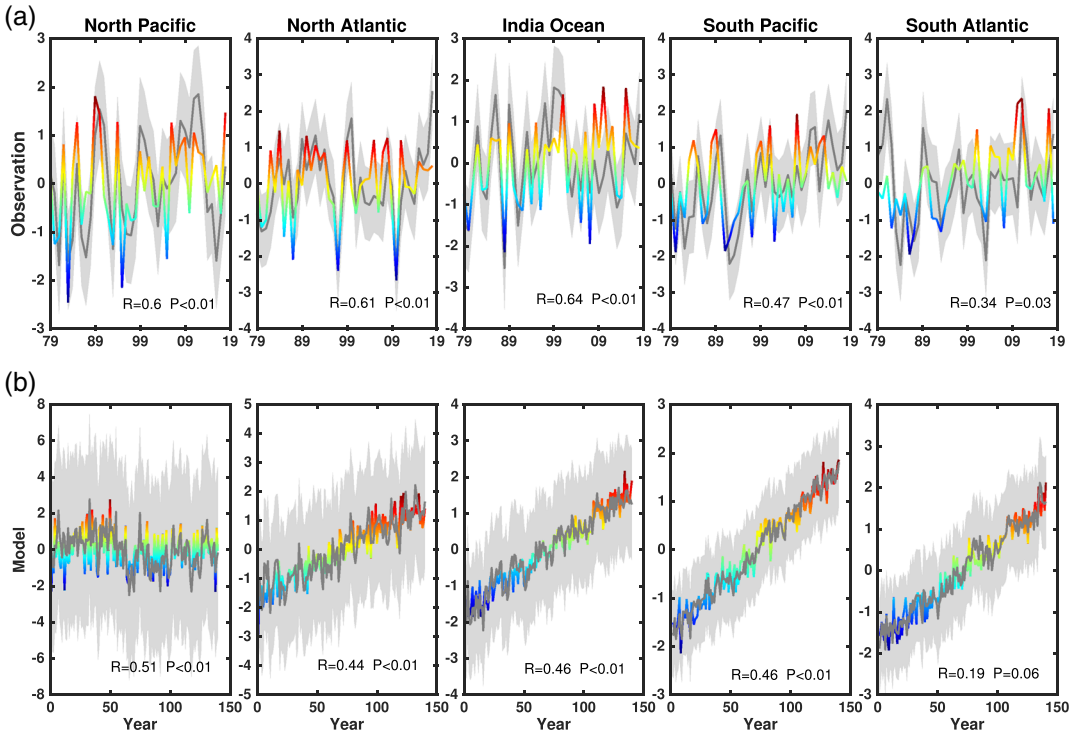


**Figure 3.** Standardized meridional variations of MMTG (gray lines) and width of tropics (colored lines) in different ocean basins. Positive values mean poleward shift, and negative values indicate equatorward contraction. The detrended correlation coefficients between the two indices and their corresponding *P* value (Student's *t* test) are given at the bottom of each panel, respectively. The gray shading shows the standard deviation of meridional variations of MMTG. (a) Observational results based on ERA5 and HadISST data sets. (b) Multimodel ensemble results based on the 140 years of the 1ptCO2 experiment from the CMIP5. Here, the R and P are multimodel ensemble mean values.

In addition to observational data, the piControl and 1pctCO2 experiments from the Coupled Model Intercomparison Project Phase 5 (CMIP5) (Taylor et al., 2012) are used as well. Twenty-four climate models are included to obtain an ensemble mean result. Detailed information on the models we use is summarized in Table 1.

To further disentangle the effect of ocean-atmosphere dynamic coupling, we carry out four sets of sensitivity experiments with the Finite Element Sea Ice-Ocean Model (FESOM, Wang et al., 2014) and the atmospheric general circulation model ECHAM6 (Giorgetta et al., 2013). These experiments are introduced in sections 4–6, where their results are discussed.

## 3. Coupling Between Tropical Width and Meridional Variations of MMTG

A fundamental driver of the atmospheric circulation is the meridional temperature gradient. Tropical expansion is associated with a poleward displacement of westerlies, jet streams, and storm tracks (Archer & Caldeira, 2008; Chen et al., 2008; Yin, 2005). These phenomena are all associated with the atmospheric meridional temperature gradients (Kaspi & Flierl, 2007; Lesieur et al., 2000; Sampe et al., 2010; Yang et al., 2019), raising the question of whether the displacement of the meridional temperature gradient is associated with the tropical width.

Given that the tropical width does not vary homogeneously over all ocean basins (Amaya et al., 2018), we examine the tropical width from a regional perspective. The annual-mean tropical width over an individual ocean basin is calculated as a metric of the latitude where the near-surface zonal wind changes from easterly to westerly in the subtropics (USF, see section 2). To get the corresponding pattern of SST gradient related to the wider tropics, we regress the USF indices of tropical width onto a field of absolute value of meridional SST gradients over their corresponding ocean basins (Figure 1). Both observations and model results from the CMIP5 exhibit a decrease of SST gradient over the latitude band between 25° and 40°, while an

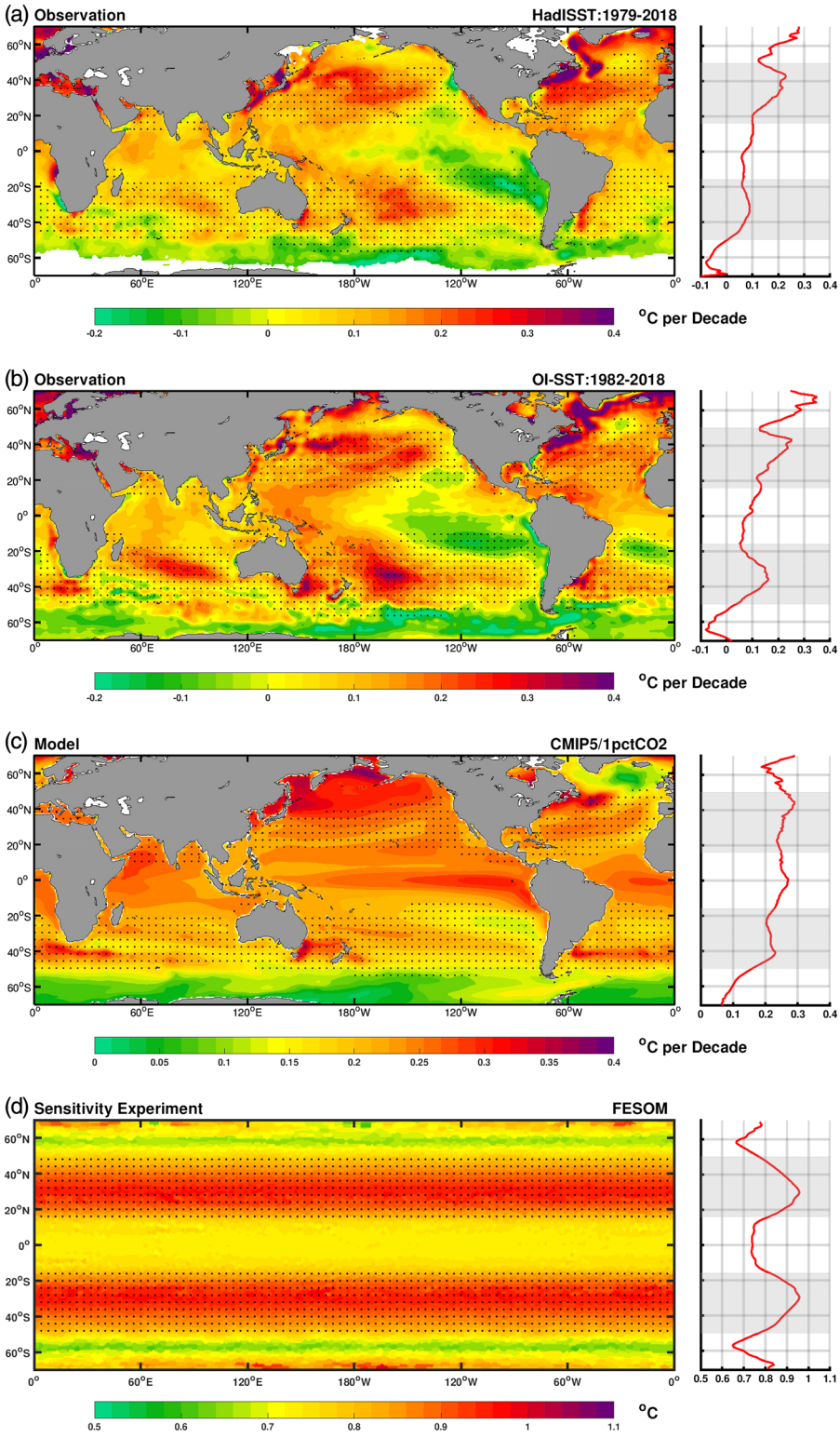


**Figure 4.** Observational and simulated linear trend of SST. The stippled area shows the subtropical convergence zone based on wind stress curl (Figure 5a). The right panels show the zonal mean of the SST anomaly with the subtropical convergence zone highlighted by gray shading. (a) Observational results based on HadISST covering 1979–2018. (b) Observational results based on OISST covering 1982–2018. (c) Multimodel ensemble results based on the 140 years of the 1ptCO2 experiment from CMIP5. (d) SST anomaly under forcing of 1°C uniform surface warming. The result is based on an oceanic sensitivity experiment conducted with a simplified aqua-planet setup of FESOM (see last paragraph of section 4).

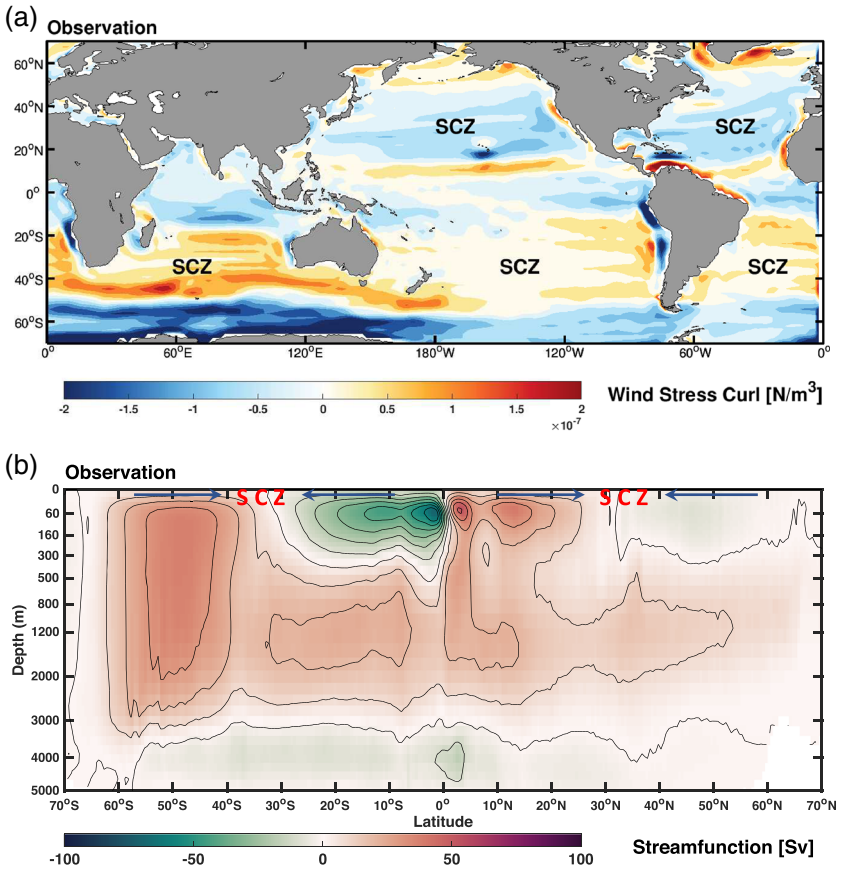


**Figure 5.** The subtropical convergence zones (SCZs) illustrated from horizontal (a) and vertical (b) point of views. (a) Climatological pattern of ocean surface wind stress curl. The SCZs are shown by the negative/positive wind stress curl over the subtropical Northern/Southern Hemispheres. Result based on the climatology near-surface ocean wind between 1979 and 2018. (b) Climatological streamfunction of globally meridional overturning circulation. Positive values indicate clockwise flow, and negative values stand for anticlockwise flow. The thick black arrows illustrate the main features of surface currents. The red text shows the position of SCZ. The results are based on SODA reanalysis covering 1948–2008.

increase of SST gradient is found over the latitude band between 40° and 55°. Such features are notable across all ocean basins. The pattern illustrates that the wider tropics are linked to poleward displacement of the meridional SST gradient over the midlatitude area, that is, MMTG.

We estimate the meridional variations of MMTG by calculating the median latitudinal position of meridional SST gradients between 25° and 55° (see Equation 1). The resultant time series is then regressed onto the near-surface zonal wind, which is one of the parameters to identify tropical width. The results (Figure 2) show that poleward displacement of the MMTG corresponds to a widespread easterly (westerly) wind anomalies over the latitude band between 20° and 45° (50–70°). This pattern indicates that poleward shift of MMTG is intimately related to a poleward shift of the near-surface winds, a typical feature of wider tropics.

We compare the indices of the MMTG with the tropical width in all ocean basins. As shown in Figure 3a, variations of the tropical width and MMTG share very similar temporal evolutions, that is, wider tropics corresponds to a poleward shift of the regional MMTG, and vice versa. We notice that both indices show positive trends, in particular over the Southern Hemisphere, implying that the edge of the tropics and the position of the MMTG have moved toward higher latitudes during the past four decades.

The coherence between the tropical width and MMTG (Figures 1–3) suggests that they are strongly coupled. On one hand, Yang et al. (2020) pointed out that the shift of the near-surface wind associated with tropical expansion drives a poleward migration of the large-scale ocean gyres, contributing to a displacement of the subtropical front (the sharpest temperature gradient in midlatitude) toward higher latitudes. On the other hand, SST gradients have been demonstrated to be a powerful forcing in anchoring the location of the westerly jet and midlatitude circulation (Hudson, 2012; Nakamura et al., 2004; Sampe et al., 2010). The coupled

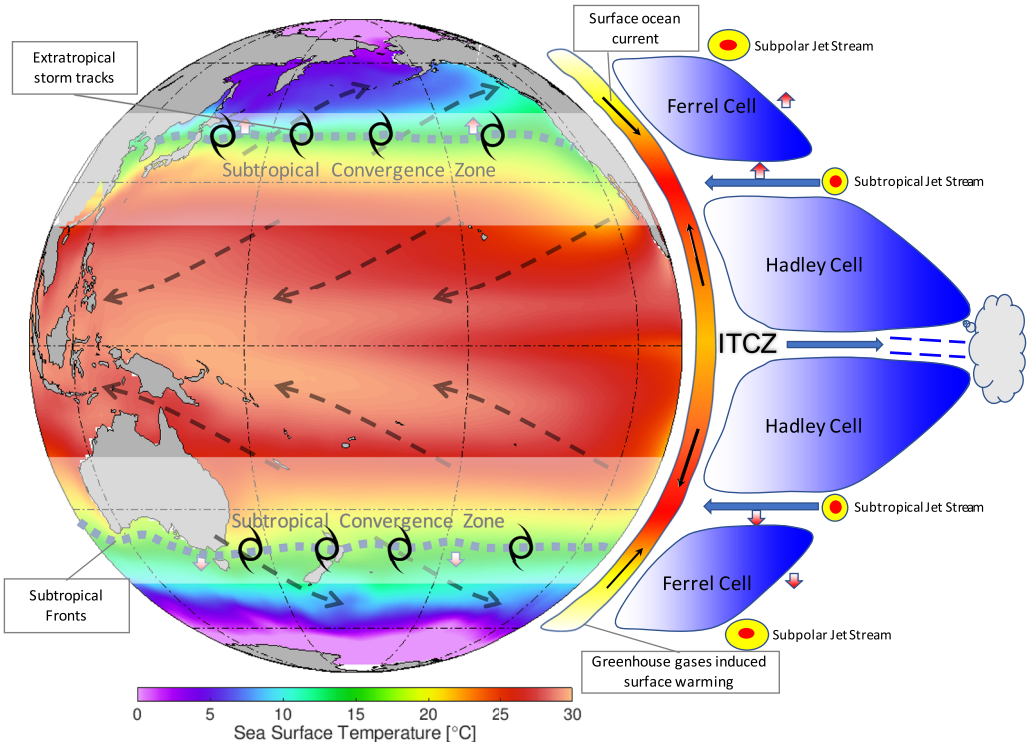


**Figure 6.** Schematic diagram explaining tropical expansion. The shading indicates the sea surface temperature, the black dashed arrows illustrate the near surface winds, the white patches are the subtropical convergence zones, and the thick gray dashed lines represent the subtropical fronts. The deep tropical heating maintains the rising branch of the Hadley circulation, namely, the ITCZ. The upper airflow losses buoyancy when it is cooled by radiative cooling, generating the sinking branch of the Hadley circulation near the subtropics. Under the forcing of trade and westerly winds, the subtropical ocean is a zone of convergence of the surface water. Therefore, greenhouse gas-induced radiative forcing produces more warming over the subtropical convergence zone. Such warming pushes the midlatitude meridional temperature gradient and associated storm tracks, jet streams, and descending branch of Hadley circulation toward higher latitudes.

ocean-atmosphere dynamics raises a new question as to whether the poleward displacement of oceanic MMTG initially drives the atmospheric tropical expansion, or vice versa.

## 4. Poleward Advancing of the MMTG Under Global Warming

To address the above question, we explore the response of the MMTG to global warming based on the 1pctCO2 experiment from the CMIP5, in which the concentration of GHG increases 1% per year until it has quadrupled. Figure 3b presents the variations of the MMTG and tropical width in the 1pctCO2 experiment. Similar to observations (Figure 3a), the multimodel ensemble results indicate that the edge of the tropics largely follows the meridional variations of MMTG, not only on an interannual timescale, but also for the long-term trend. It is worth emphasizing that the close correlation between the MMTG and the tropical width is also notable in other CMIP5 experiments, such as the piControl, abrupt4×CO2, and RCP8.5 experiments (not shown). We notice that most of the MMTG are migrating toward higher latitudes under GHG forcing, except over the North Pacific Ocean, where the models simulate a relatively stationary MMTG and tropical width (for reasons to be elaborated later).

To understand the reason for the poleward displacement of the MMTG, we examine the SST trends in observations and climate model simulations (Figure 4). A relatively faster surface warming over the subtropical regions of the Pacific and the Atlantic Oceans are found over both hemispheres (Figure 4a, based on HadISST, covering 1979–2018). Considering that the SST data before the satellite era are reconstructed with relatively sparse observations, we cross validate the HadISST result with the satellite-based data set OISST. Similarly, the OISST, covering 1982–2018, illustrates a relatively faster surface warming over the subtropical regions of all ocean basins, including the Indian Ocean (Figure 4b). These subtropical regions with enhanced warming trend coincide with the SCZ (Figure 5), where the easterly winds and westerly winds converge the

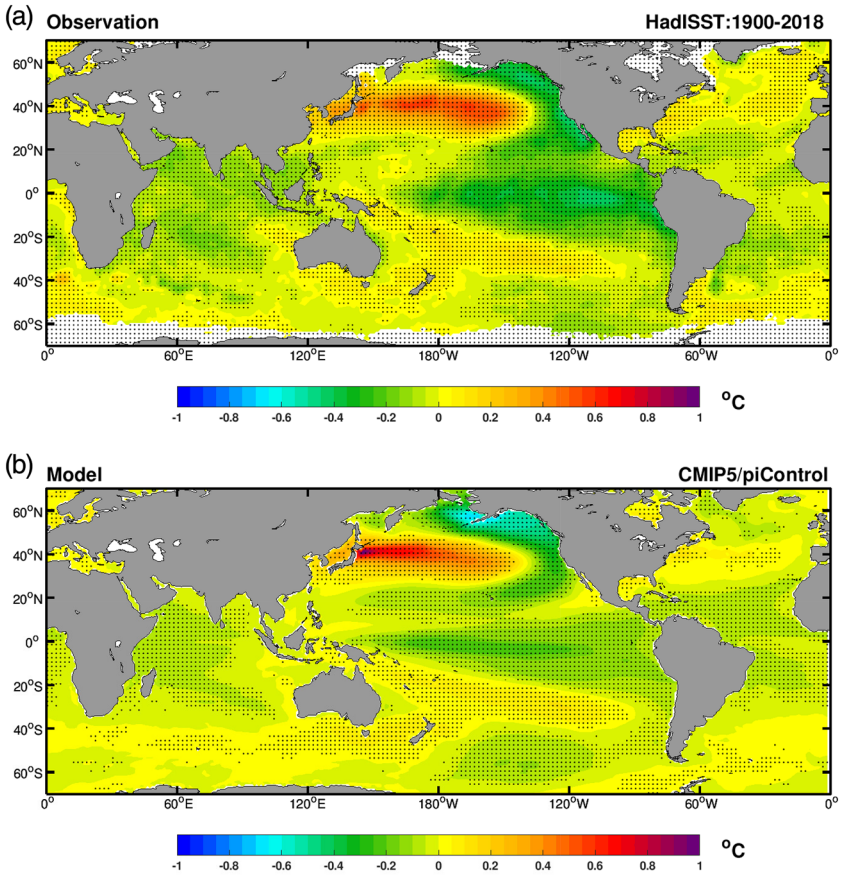


**Figure 7.** Signature of negative phase of Pacific Decadal Oscillation (PDO). Results are obtained by regressing the standardized PDO index against the sea surface temperature. (a) Observational result based on HadISST (1900–2018). Stippling indicates regions where the regression passes the 95% confidence level (Student's *t* test). (b) Multimodel ensemble (24 models) result based on the last 100 years of CMIP5/piControl experiment. Stippling indicates regions where more than 75% of the models agree on the sign of the regression values. The PDO index is defined as the first principal component of empirical orthogonal function (EOF) analysis of the monthly SST data over the North Pacific Ocean (poleward of 20°N).

surface water via Ekman transport. It is worth noting that, previously, a similar enhanced subtropical warming has also been detected in the troposphere (Fu et al., 2006), a layer where the ocean and atmosphere are closely coupled.

Compared with observations (Figures 4b and 4c), the SST pattern under GHG forcing shows similar enhanced surface warming over the subtropical oceans (except over the North Pacific Ocean). The enhanced subtropical warming leads to a reduction/increase in the meridional temperature gradient over low/high latitudes. Consequently, the MMTG is shifted toward the poles. Over the North Pacific Ocean, the simulated strongest warming occurs over the subpolar ocean instead of the subtropical ocean (Figure 4c), likely due to the retreat of Arctic sea ice (Deser et al., 2015). Such a pattern reduces the overall meridional SST gradients over the Northern Pacific Ocean (not shown). However, the position of the MMTG remains relatively stable (as shown in Figure 3b, the North Pacific section).

According to the Ekman transport theory, both the low-latitude easterly wind and the midlatitude westerly wind contribute to transporting the upper ocean water toward the SCZ. Therefore, the SCZ is a band of convergence of surface water (Figure 5). These SCZs are also known as regions where floating marine debris is accumulating (Eriksen et al., 2014). For the same reason, we propose that under global warming, the subtropical ocean also accumulates surface heat and experiences more warming due to mean Ekman convergence (Figures 5 and 6).

As the observed SST trends over the Pacific Ocean resemble the signature of the negative phase of PDO (Figure 7), they were previously interpreted as internal climate variability (Allen et al., 2014; Allen &

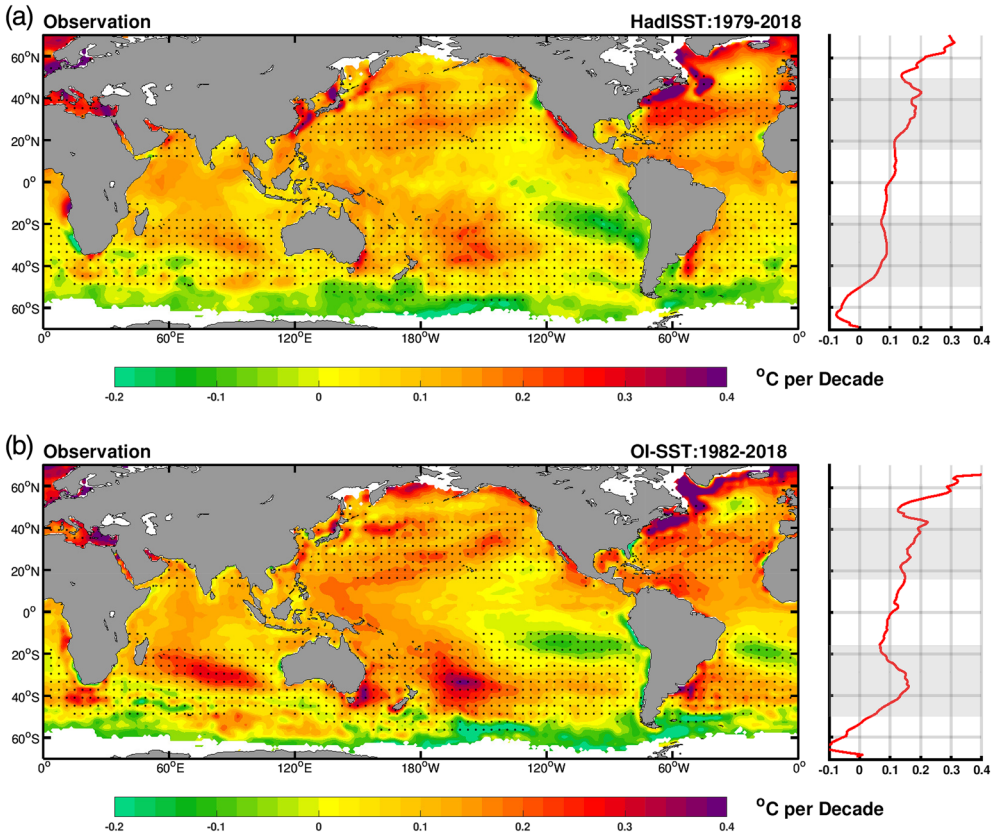


**Figure 8.** (a, b) Observational linear trend of sea surface temperature after removing the signal of Pacific Decadal Oscillation (PDO). The PDO signal is identified and removed from the original SST records by performing a linear regression of the SST variability with respect to the PDO index. A similar approach has also been applied by Ionita et al. (2014). The stippling area locates the subtropical convergence zone according to the pattern of wind stress curl (Figure 5a).

Kovilakam, 2017; Grise et al., 2019; Mantsis et al., 2017; Tandon & Cane, 2017). However, we notice that the negative phase of PDO only manifests warming over the subtropical Pacific Ocean, which is not consistent with the fact that the observed subtropical warming occurs in all ocean basins in both hemispheres. More importantly, the enhanced subtropical ocean warming still remains even if the PDO signal is removed (Figure 8) or during a positive phase (2014–2018) of PDO (Figure 9). These facts suggest that part of the enhanced warming over the SCZ is independent from the fluctuations of PDO. As we suggested, the background convergence of surface warmed water can lead to enhanced warming of the SCZ under global warming.

To verify our hypothesis, we conduct a set of sensitivity experiments using a simplified aqua-planet setup with FESOM (Wang et al., 2014). In this simplified setup, the ocean is forced only by surface air temperature and zonal surface wind (no seasonality). The net ocean surface heat flux is prescribed as $SAT - SST$, in which $SAT$ is the prescribed surface air temperature and $SST$ is the sea surface temperature. The ocean has a uniform 4,000 m water depth and a uniform salinity of 34 PSU. The control run is integrated for 1,200 years using the prescribed surface air temperature and zonal surface wind forcing (Figure 10). The sensitivity simulation is initialized from the 1,000th year of the control run and integrated for 200 years using a spatially and temporally uniform forcing of 1°C warmer surface air temperature (wind forcing is the same as the control run). The last 100 years of the sensitivity simulation is used to compare with the last 100 years of the control run. As shown in Figure 4d, even though the surface air temperature forcing is uniform, the increase in SST is not. The SCZ warms faster than other regions due to background Ekman convergence. The enhanced warming over the subtropical oceans expand the tropical warm water zone, leading to a

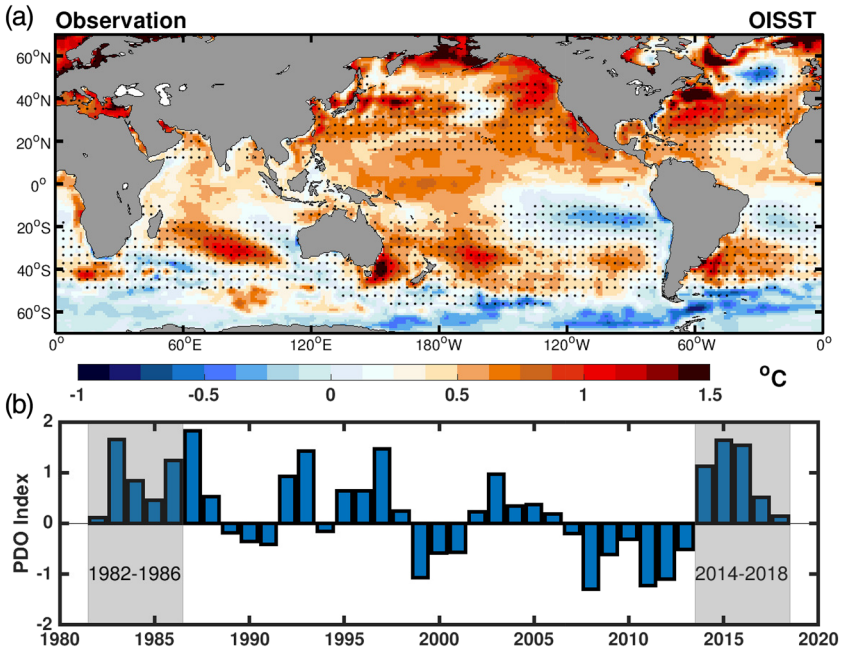


**Figure 9.** (a) Observational SST anomaly during the last 5 years of the satellite era (2014–2018, positive phase of PDO) referenced to the first 5 years of the satellite era (1982–1986). (b) Index of the Pacific Decadal Oscillation (PDO). An enhanced subtropical warming pattern appears over all the ocean basins, corresponding to the subtropical convergence zone illustrated by the stippling area.

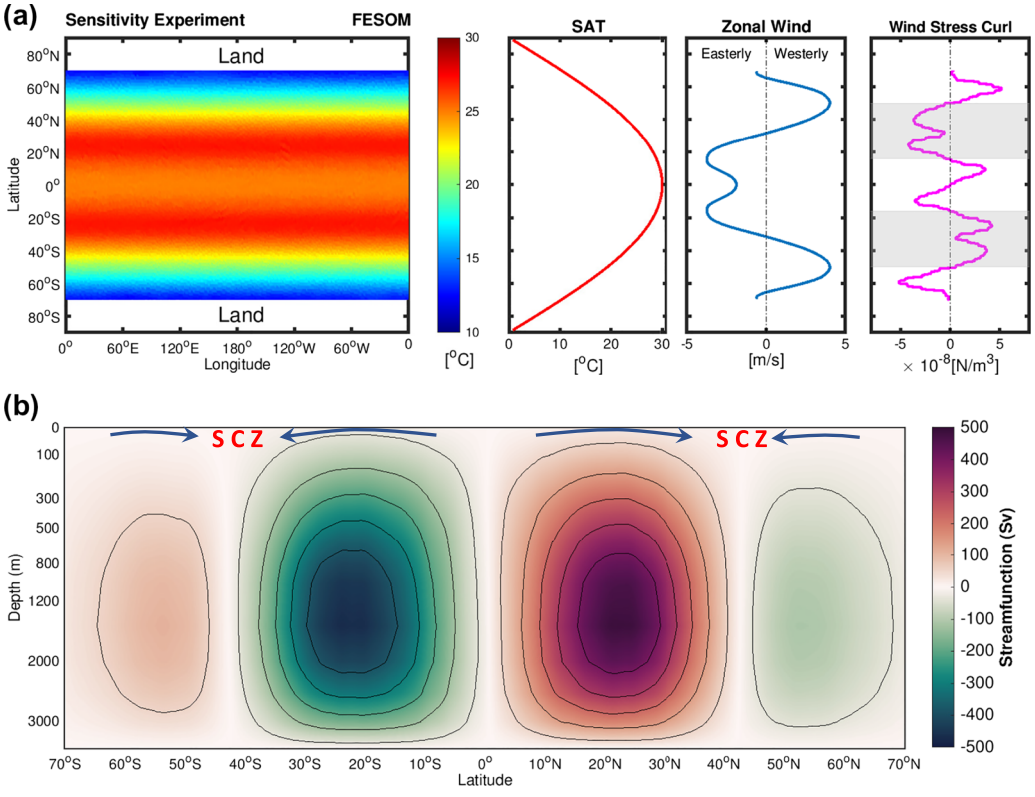


**Figure 10.** Climatology conditions simulated by a simplified aqua-planet setup of FESOM. Results based on the last 100 years of climatology conditions in the control run. (a) sea surface temperature (left), forcing of surface air temperature (middle-left), near surface wind (middle-right), and wind stress curl (right). Gray shading area in the right panel marks the subtropical convergence zone. (b) Climatological streamfunction of global meridional overturning circulation. Positive values indicate clockwise flow, and negative values stand for anticlockwise flow. The thick black arrows illustrate the main features of surface currents. The red texts show the location of the SCZ.

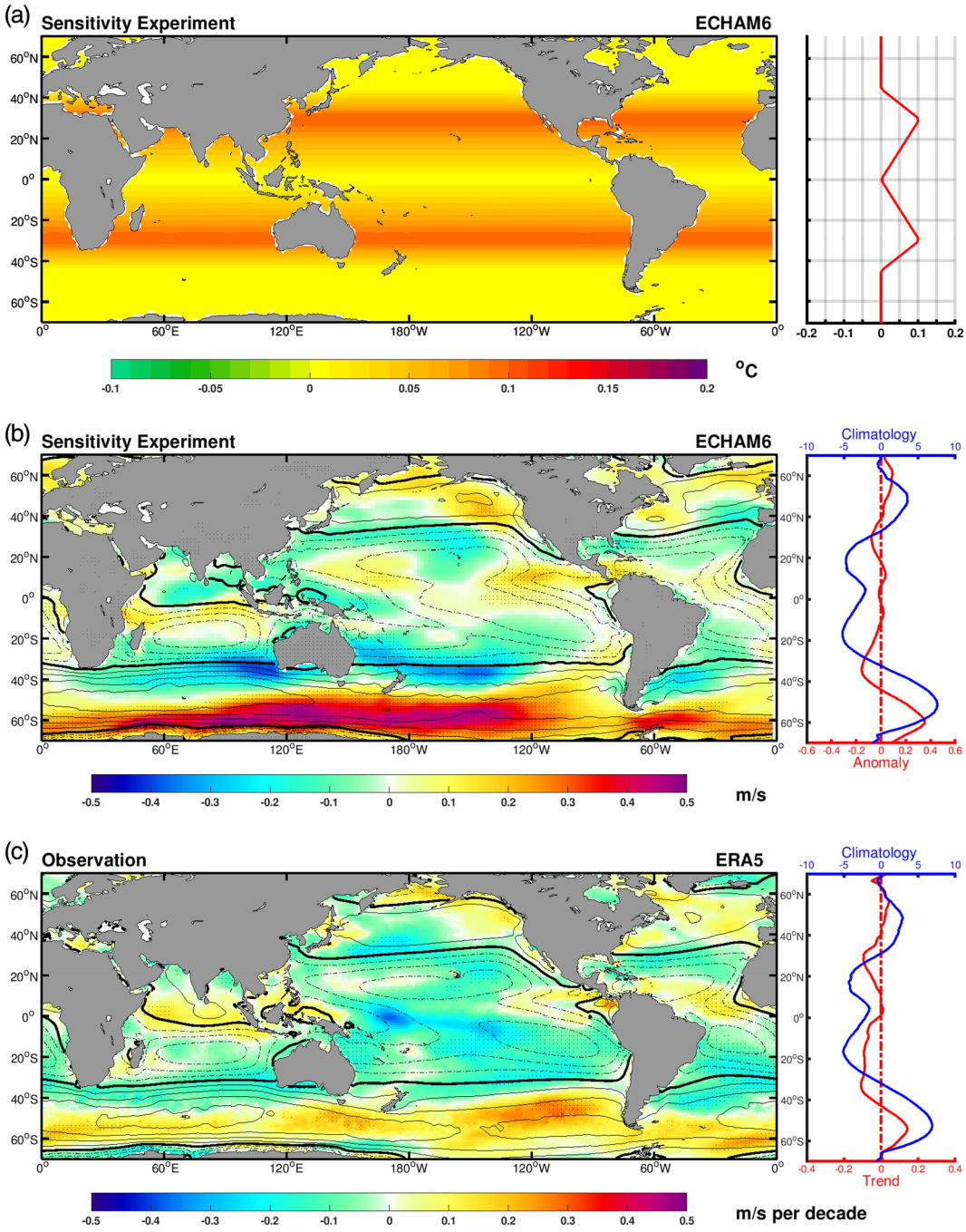


**Figure 11.** Tropical expansion driven by poleward shift of midlatitude meridional temperature gradients (or enhanced subtropical warming). (a) Idealized SST anomaly applied in the ECHAM6 sensitivity simulation. The right panel shows the zonal mean profile of the SST anomaly. (b) Pattern of near-surface zonal wind anomaly under increasing SST forcing over the subtropical region (Figure 11a). Results based on ECHAM6 atmospheric sensitivity simulation. Stippling denotes regions where the anomalies are significant (Student's *t* test). (c) Observational trend of near-surface zonal wind. Results based on the ERA5 data covering 1979–2018. Stippling indicates regions where the trends pass the 95% confidence level (Student's *t* test). The right panels in (b) and (c) present the zonal mean profiles of climatology (blue) and trend (red) of zonal near-surface wind.

poleward advance of the MMTG. Our aqua-planet experiment illustrates that the poleward advance of the MMTG occurs primarily due to the background ocean circulation, which is independent from the changes in atmospheric circulation (as the wind forcing remained the same in the two simulations).

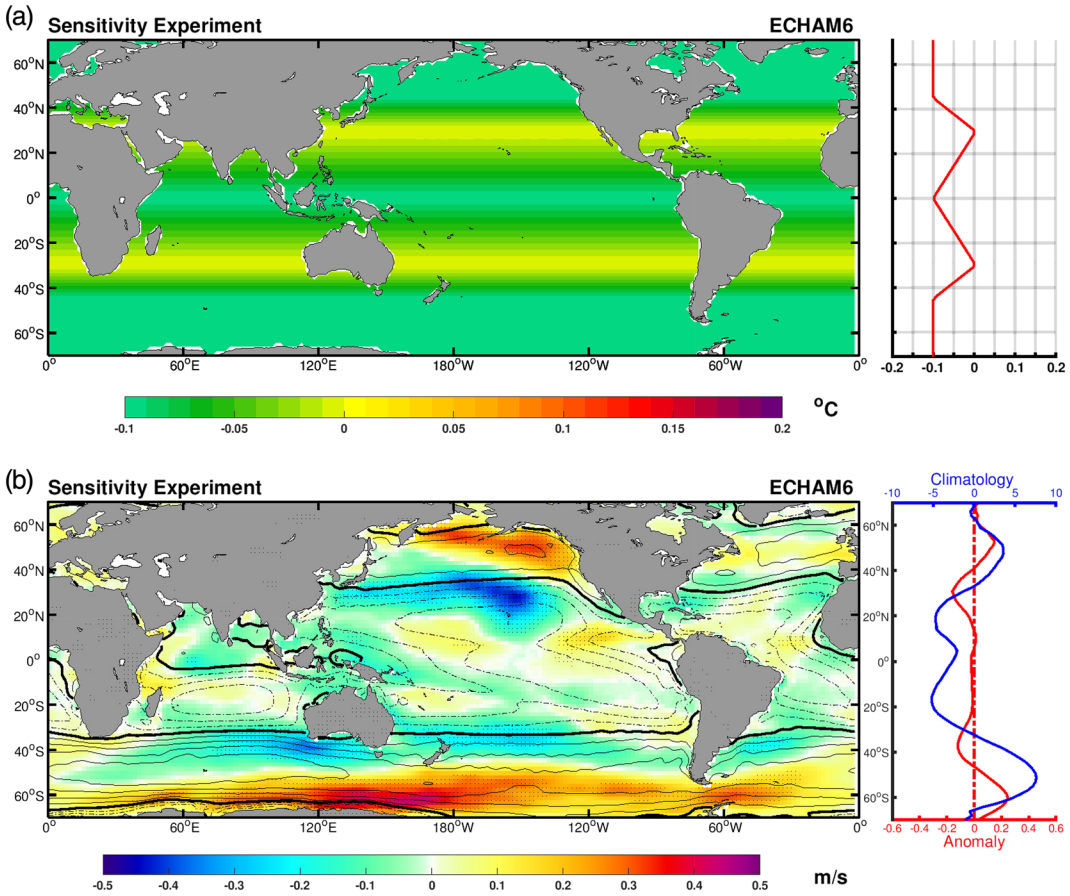


**Figure 12.** Tropical expansion driven by poleward shift of midlatitude meridional temperature gradients under a global cooling condition. (a) Idealized SST anomaly applied in the ECHAM6 sensitivity simulation. The right panel gives the zonal mean SST anomaly. (b) Zonal wind anomaly obtained in the sensitivity simulation. The right panel gives the zonal mean climatology (blue) and anomaly (red) of zonal wind. Stippling indicates regions where the anomalies pass the 95% confidence level (Student's *t* test). Note that in this setup, there is global cooling signal, but the tropics still expands due to relative warmer SST over the subtropical ocean.

## 5. Tropical Expansion Driven by Enhanced Subtropical Warming

To examine whether the enhanced subtropical ocean warming and the associated poleward shift of the oceanic MMTG are able to drive wider tropics, we carried out a sensitivity experiment using the atmospheric model ECHAM6 (Giorgetta et al., 2013). In the control run, we force the atmosphere using climatological SST (1979–2008), while the sensitivity simulation is conducted by introducing a slightly warmer SST (0.1 K) over the subtropical ocean (Figure 11a). With a 0.1 K SST warming over the subtropical ocean (Figure 11a), the meridional SST gradient is reduced over the low latitudes while enhanced over the high latitudes. Hence, the MMTG is artificially shifted toward higher latitudes. Both simulations are integrated for 150 years, and the last 100 years are used for analysis. The results show that warmer SST over the subtropical ocean is able to drive the tropical expansion resembling that seen in observations (Figures 11b and 11c). Sensitivity simulations carried out by other atmospheric models also confirmed that the width of Hadley circulation is sensitive to the subtropical SST anomaly (Brayshaw et al., 2008; Chen et al., 2010; Tandon et al., 2013; Zhou et al., 2020), suggesting that our results are not model dependent.

Some previous studies suggested that raising global mean temperature contributes to expanding the tropics (Frierson et al., 2007; Medeiros et al., 2015; Son et al., 2018; Staten et al., 2014). The above sensitivity simulation introduces an additional signal of increased global mean temperature, which might also be the cause of expanding tropics. To exclude such a possibility, we perform another sensitivity simulation by shifting the MMTG under a global cooling condition. This approach is achieved by introducing an SST cooling of

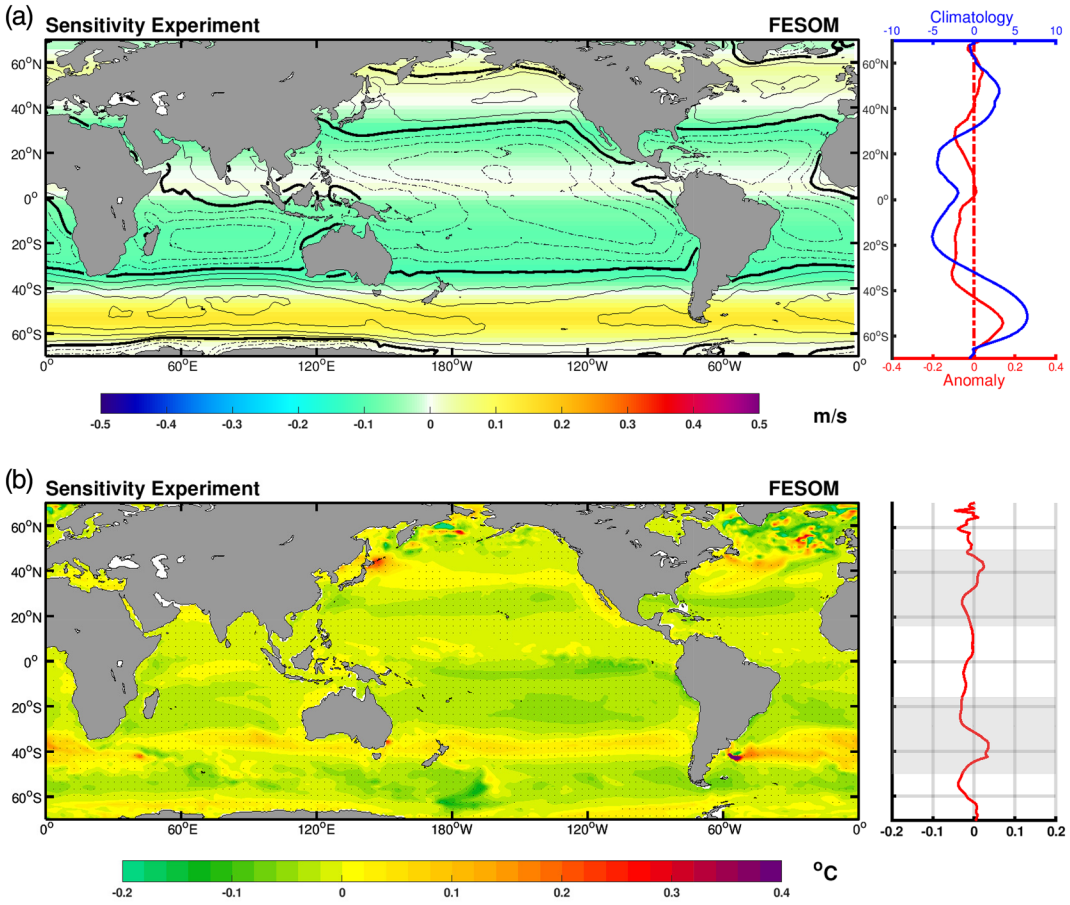


**Figure 13.** Sensitivity simulation of SST anomaly under forcing of poleward shift of surface wind. (a) Zonal surface wind anomaly applied in the sensitivity simulation. The right panel gives the zonal mean climatology (blue line) and anomaly (red line) of wind. (b) SST anomaly under forcing of shifting wind. The right panel gives the zonal mean SST anomaly (red). Results are based on sensitivity experiment carried out by FESOM. Stippling denotes regions where the anomalies are significant (Student's *t* test).

−0.1 K globally, except that over the midlatitude (Figure 12a). In this setup, the global mean temperature is reduced, while the signal of shifting MMTG remains. Again, the sensitivity simulation is integrated for 150 years, and the last 100 years are used for analysis. As shown in Figure 12b, the widening of the tropics still persists despite the global cooling condition, indicating the potency of the temperature gradient in driving the atmospheric circulation response.

## 6. Responses of SST to Tropical Expansion

The above two sets of experiments explore the response of atmospheric circulation to SST changes. Considering that the atmosphere and the ocean are closely coupled, it is interesting to examine how the SST responds to tropical expansion. Here, we carried out one more sensitivity experiment using the ocean model FESOM (Wang et al., 2014). The control run is forced with climatology (1948–1999) atmospheric forcing based on the CORE-II data sets (Large & Yeager, 2009). The sensitivity simulation is the same as the control run, except for adding a zonal wind anomaly (Figure 13a) resembling the tropical expansion indicated by the observations (according to the zonal mean wind trend based on Figure 11c). The control run is integrated for 100 years, and the sensitivity simulation runs for 50 years initialized from the 50th year of the control run. We compare the last 10 years of both simulations. As shown in Figure 13b, poleward displacement of surface winds (wider tropics) leads to a cooling/warming over the equatorial/polar flanks of SCZ. This is primarily because the shift in wind helps to shift the major ocean gyres (Yang et al., 2020) and transport more heat from lower latitudes toward higher latitudes. This experiment suggests that wider tropics

cannot produce subtropical warming that seen in observations. Instead, it plays a secondary role in modifying the enhanced subtropical warming induced by the convergence of surface water.

We propose that under global warming, the SCZ experiences more warming due to mean Ekman transport. The enhanced subtropical warming and associated poleward advance of the MMTG drives the tropical expansion and shift the atmospheric winds, jet streams, and storm tracks toward poles (Figure 6). The displacement of atmospheric winds, in turn, forces a poleward shift of the wind-driven ocean circulation and causes a migration of the oceanic subtropical front toward higher latitudes (Fyfe et al., 2007; Yang et al., 2020). The migration of the subtropical front further shift the MMTG toward poles, activating a positive feedback. Due to the coupled ocean-atmosphere feedback, the final maximum subtropical warming, equilibrated with ocean changes, occurs not at the center of the background SCZ, but slightly at the polar flank of the SCZ (Figures 4a–4c).

## 7. Discussion and Conclusions

The Hadley circulation is driven by the uneven meridional heating between the tropics and the subtropics. Held (2000) proposed that the edge of the tropics is determined by the latitude where baroclinic instability becomes sufficiently strong so that baroclinic eddies break out to terminate the angular momentum conservation regime of the zonal wind. The baroclinicity ties strongly to the temperature gradients, affecting the jet streams, storm tracks, and westerlies (Kaspi & Flierl, 2007; Lesieur et al., 2000). Under global warming, the enhanced subtropical warming operates at the proximity of the largest atmospheric baroclinic instability and serves as a factor for reducing the subtropical temperature gradient, pushing the MMTG and baroclinic instability poleward. The warming over the subtropical region, therefore, shifts the edge of the Hadley Cell (i.e., the latitude where baroclinic instability becomes significantly strong) toward higher latitudes (Figure 6). The expansion of the Hadley Cell and the associated shift in wind in turn drive a poleward shift of the major ocean gyres and the subtropical fronts (Yang et al., 2020). This ocean response further shifts the MMTG poleward (Figure 13) and promotes the shift in atmospheric circulation.

Under the forcing of observational aerosols and ozone, climate models also produce tropical expansion (Allen et al., 2012; Polvani et al., 2011; Thompson et al., 2011). By absorbing radiation over different wavelength bands, the black carbon aerosols and ozone have a similar radiative heating effect to $CO_2$. However, unlike $CO_2$, which has an almost uniform spatial distribution, the distribution of aerosols and ozone strongly varies spatially. Increasing black carbon aerosol and tropospheric ozone over midlatitudes introduces a heating effect over the midlatitudes (Allen et al., 2012), which has the potential to reduce the local baroclinicity and sustain a poleward shift of atmospheric MMTG. The stratospheric ozone depletion over the Antarctic cools the stratosphere (Orr et al., 2012; Randel & Wu, 1999; Thompson et al., 2011) and reduces the downward longwave radiation into the troposphere. Eventually, the ozone depletion over the Antarctic maintains steeper high-latitude north-south temperature gradients (Grise et al., 2009) and causes the migration of the MMTG and associated jet stream and westerlies toward higher latitudes. Therefore, we argue that the shift in MMTG is also the key factor for the Hadley Cell expansion under forcing of aerosols and ozone. By testing $CO_2$ forcing at different latitude bands, Shaw and Tan (2018) also found that the subtropical warming centered around 30° latitude provides the largest contribution to the tropical expansion. Very likely, the same MMTG mechanism also operates in their case.

Previous studies indicate that tropical expansion has strong regional dependence (Chen et al., 2014; Grise et al., 2018; Kim et al., 2017; Lucas & Nguyen, 2015; Staten et al., 2019). We find that the regional characteristics of tropical expansion are primarily determined by the regional variations of the MMTG (Figure 3). Under forcing of increasing GHG and increasing SST, the CMIP5 1pctCO2 experiment does not project wider tropics over the North Pacific Ocean (Figure 3b). Such an exception provides an example showing that the GHG and increasing mean temperature are not the most efficient element to drive tropical expansion. Instead, our results illustrate that the meridional displacement of MMTG are strongly coupled with the width of the tropics, providing an explanation for the regional dependence of widening tropical belt.

On seasonal time scale, the edge of the tropics and associated storm tracks, westerlies, and jet streams migrate toward higher latitude during summer and vice versa during winter, primarily following the MMTG, induced by solar irradiance. On interannual to interdecadal time scales, the El Ni˜n o-Southern Oscillation (ENSO) and PDO are suggested to be related to the tropical expansion (Allen & Kovilakam,

2017; Allen et al., 2014; Grassi et al., 2012; Grise et al., 2018, 2019; Lu et al., 2008; Lucas & Nguyen, 2015; Mantsis et al., 2017; Nguyen et al., 2013; Tandon & Cane, 2017; Zhou et al., 2020). The negative phase of PDO/ENSO features warming over the subtropics, resulting in a poleward expansion of the MMTG and the tropical belt. The opposite is true for the positive phase of PDO/ENSO. From a paleoclimate perspective, the tropics are narrower during glacial periods (Son et al., 2018). This is likely the result of high-latitude sea ice and cold water advancing toward lower latitudes (Annan & Hargreaves, 2013), giving rise to an equatorward contraction of the MMTG.

During 1979–2013, the PDO underwent an overall negative trend (Figure 9b), and this trend has been argued to be responsible for the observed tropical expansion (Allen & Kovilakam, 2017; Grassi et al., 2012; Grise et al., 2019; Mantsis et al., 2017; Tandon & Cane, 2017). Since the PDO itself is an internal mode of climate variability, many studies suggested that the trend of the tropical expansion during the recent few decades is largely a part of natural climate variability (Allen & Kovilakam, 2017; Allen et al., 2014; Grassi et al., 2012; Grise et al., 2018, 2019; Lucas & Nguyen, 2015; Mantsis et al., 2017; Nguyen et al., 2013; Tandon & Cane, 2017). However, our analysis of observations, CMIP5, and aqua-planet sensitivity simulations (section 4) suggests that the observed enhanced warming over the subtropical ocean contains a component of first-order response to global warming as a result of background convergence of surface water, independent of the PDO. The enhanced subtropical warming shifts the MMTG and drives the tropical expansion. Therefore, it is plausible that global warming may have already significantly contributed to the observed tropical expansion, especially over the ocean-dominant Southern Hemisphere.

**Acknowledgments**

This work was supported in part through grant Global sea level change since the Mid Holocene: Background trends and climate-ice sheet feedbacks from the Deutsche Forschungsgemeinschaft (DFG) as part of the Special Priority Program (SPP)-1889 "Regional Sea Level Change and Society" (SeaLevel). J. L. is supported by the U.S. Department of Energy Office of Science Biological and Environmental Research as part of the Regional and Global Model Analysis program. We acknowledge furthermore the JPI-Belmont-funded PACMEDY program BMBF 01LP1607A. We would also like to acknowledge three anonymous reviewers for providing constructive comments. We thank Christian Stepanek for the help in generating the mesh for the aqua-planet FESOM setup. We acknowledge Xianyao Chen and Longjiang Mu for helpful discussion and Yongyun Hu for providing a pre-review of this manuscript. We acknowledge the World Climate Research Programme's Working Group on Coupled Modelling, which is responsible for CMIP5, and we thank the climate modeling groups (listed in Table 1 of this paper) for producing and making available their model output. For CMIP, the U.S. Department of Energy's Program for Climate Model Diagnosis and Intercomparison provides coordinating support and led development of software infrastructure in partnership with the Global Organization for Earth System Science Portals. We would like to express our gratitude and appreciation to the groups who freely distribute the data sets used in this work.

## Data Availability Statement

The data sets can be accessed with the following links: HadISST (https://www.metoffice.gov.uk/hadobs/hadisst/), OISST (https://www.esrl.noaa.gov/psd/data/gridded/data.noaa.oisst.v2.html), ERA5 (https://www.ecmwf.int/en/forecasts/datasets/reanalysis-datasets/era5), CMIP5 (https://esgf-node.llnl.gov/search/cmip5/), and PDO index (https://www.ncdc.noaa.gov/teleconnections/pdo/). The FESOM and ECHAM6 codes are publicly available from https://fesom.de/models/fesom14/ and https://www.mpimet.mpg.de/en/science/models/mpi-esm/echam/, respectively. The aqua-planet FESOM simulation is performed as described in section 4.

## References

Allen, R. J., & Kovilakam, M. (2017). The role of natural climate variability in recent tropical expansion. *Journal of Climate*, *30*(16), 6329–6350.

Allen, R. J., Norris, J. R., & Kovilakam, M. (2014). Influence of anthropogenic aerosols and the Pacific Decadal Oscillation on tropical belt width. *Nature Geoscience*, *7*(4), ngeo2091.

Allen, R. J., Sherwood, S. C., Norris, J. R., & Zender, C. S. (2012). Recent Northern Hemisphere tropical expansion primarily driven by black carbon and tropospheric ozone. *Nature*, *485*(7398), 350.

Amaya, D. J., Siler, N., Xie, S. P., & Miller, A. J. (2018). The interplay of internal and forced modes of Hadley Cell expansion: Lessons from the global warming hiatus. *Climate Dynamics*, *51*(1-2), 305–319.

Annan, J., & Hargreaves, J. C. (2013). A new global reconstruction of temperature changes at the Last Glacial Maximum. *Climate of the Past*, *9*(1), 367–376.

Archer, C. L., & Caldeira, K. (2008). Historical trends in the jet streams. *Geophysical Research Letters*, *35*, L08803. https://doi.org/10.1029/2008GL033614

Bard, E., & Rickaby, R. E. (2009). Migration of the subtropical front as a modulator of glacial climate. *Nature*, *460*(7253), 380.

Bender, F. A., Ramanathan, V., & Tselioudis, G. (2012). Changes in extratropical storm track cloudiness 1983–2008: Observational support for a poleward shift. *Climate Dynamics*, *38*(9-10), 2037–2053.

Benz, V., Esper, O., Gersonde, R., Lamy, F., & Tiedemann, R. (2016). Last Glacial Maximum sea surface temperature and sea-ice extent in the Pacific sector of the Southern Ocean. *Quaternary Science Reviews*, *146*, 216–237.

Brayshaw, D. J., Hoskins, B., & Blackburn, M. (2008). The storm-track response to idealized SST perturbations in an aquaplanet GCM. *Journal of the Atmospheric Sciences*, *65*(9), 2842–2860.

Cai, W., & Cowan, T. (2013). Southeast Australia autumn rainfall reduction: A climate-change-induced poleward shift of ocean–atmosphere circulation. *Journal of Climate*, *26*(1), 189–205.

Carton, J. A., & Giese, B. S. (2008). A reanalysis of ocean climate using Simple Ocean Data Assimilation (SODA). *Monthly Weather Review*, *136*(8), 2999–3017.

Chen, G., Lu, J., & Frierson, D. M. (2008). Phase speed spectra and the latitude of surface westerlies: Interannual variability and global warming trend. *Journal of Climate*, *21*(22), 5942–5959.

Chen, G., Plumb, R. A., & Lu, J. (2010). Sensitivities of zonal mean atmospheric circulation to SST warming in an aqua-planet model. *Geophysical Research Letters*, *37*, L12701. https://doi.org/10.1029/2010GL043473

Chen, S., Wei, K., Chen, W., & Song, L. (2014). Regional changes in the annual mean Hadley circulation in recent decades. *Journal of Geophysical Research: Atmospheres*, *119*, 7815–7832. https://doi.org/10.1002/2014JD021540

Deser, C., Tomas, R. A., & Sun, L. (2015). The role of ocean-atmosphere coupling in the zonal-mean atmospheric response to Arctic sea ice loss. *Journal of Climate*, *28*(6), 2168–2186.
Eriksen, M., Lebreton, L. C., Carson, H. S., Thiel, M., Moore, C. J., Borerro, J. C., & Reisser, J. (2014). Plastic pollution in the world's oceans: More than 5 trillion plastic pieces weighing over 250,000 tons afloat at sea. *PloS one*, *9*(12), e111913.
Frierson, D. M., Lu, J., & Chen, G. (2007). Width of the Hadley cell in simple and comprehensive general circulation models. *Geophysical Research Letters*, *34*, L18804. https://doi.org/10.1029/2007GL031115
Fu, Q., Johanson, C. M., Wallace, J. M., & Reichler, T. (2006). Enhanced mid-latitude tropospheric warming in satellite measurements. *Science*, *312*(5777), 1179–1179.
Fyfe, J. C., Saenko, O. A., Zickfeld, K., Eby, M., & Weaver, A. J. (2007). The role of poleward-intensifying winds on Southern Ocean warming. *Journal of Climate*, *20*(21), 5391–5400.
Gersonde, R., Crosta, X., Abelmann, A., & Armand, L. (2005). Sea-surface temperature and sea ice distribution of the Southern Ocean at the EPILOG Last Glacial Maximumøa circum-Antarctic view based on siliceous microfossil records. *Quaternary science reviews*, *24*(7-9), 869–896.
Giorgetta, M. A., Roeckner, E., Mauritsen, T., Bader, J., Crueger, T., Esch, M., et al. (2013). The atmospheric general circulation model ECHAM6-model description. Max Planck Institute for Meteorology.
Grassi, B., Redaelli, G., Canziani, P. O., & Visconti, G. (2012). Effects of the PDO phase on the tropical belt width. *Journal of Climate*, *25*(9), 3282–3290.
Grise, K. M., Davis, S. M., Simpson, I. R., Waugh, D. W., Fu, Q., Allen, R. J., et al. (2019). Recent tropical expansion: Natural variability or forced response? *Journal of Climate*, *32*(5), 1551–1571.
Grise, K. M., Davis, S. M., Staten, P. W., & Adam, O. (2018). Regional and seasonal characteristics of the recent expansion of the tropics. *Journal of Climate*, *31*(17), 6839–6856.
Grise, K. M., & Polvani, L. M. (2014). The response of midlatitude jets to increased $CO_2$: Distinguishing the roles of sea surface temperature and direct radiative forcing. *Geophysical Research Letters*, *41*, 6863–6871. https://doi.org/10.1002/2014GL061638
Grise, K. M., Thompson, D. W., & Forster, P. M. (2009). On the role of radiative processes in stratosphere-troposphere coupling. *Journal of climate*, *22*(15), 4154–4161.
Heffernan, O. (2016). The mystery of the expanding tropics. *Nature News*, *530*(7588), 20.
Held, I. (2000). The general circulation of the atmosphere, 2000 program of study in geophysical fluid dynamics (*3*): Woods Hole Oceanogr. Inst. Tech. Rep. WHOI-2001.
Hersbach, H., Bell, B., Berrisford, P., Horányi, A., Sabater, J. M., Nicolas, J., et al. (2019). Global reanalysis: goodbye ERA-Interim, hello ERA5. *ECMWF Newsl*, *159*, 17–24.
Hu, Y., & Fu, Q. (2007). Observed poleward expansion of the Hadley circulation since 1979. *Atmospheric Chemistry and Physics*, *7*(19), 5229–5236.
Hu, Y., Huang, H., & Zhou, C. (2018). Widening and weakening of the Hadley circulation under global warming. *Science Bulletin*, *63*(10), 640–644.
Hu, Y., Tao, L., & Liu, J. (2013). Poleward expansion of the Hadley circulation in CMIP5 simulations. *Advances in Atmospheric Sciences*, *30*(3), 790.
Hudson, R. (2012). Measurements of the movement of the jet streams at mid-latitudes, in the Northern and Southern Hemispheres, 1979 to 2010. *Atmospheric Chemistry and Physics*, *12*(16), 7797–7808.
Ionita, M., Felis, T., Lohmann, G., Rimbu, N., & Pätzold, J. (2014). Distinct modes of East Asian Winter Monsoon documented by a southern Red Sea coral record. *Journal of Geophysical Research: Oceans*, *119*, 1517–1533. https://doi.org/10.1002/2013JC009203
Johanson, C. M., & Fu, Q. (2009). Hadley cell widening: Model simulations versus observations. *Journal of Climate*, *22*(10), 2713–2725.
Kaspi, Y., & Flierl, G. R. (2007). Formation of jets by baroclinic instability on gas planet atmospheres. *Journal of the Atmospheric Sciences*, *64*(9), 3177–3194.
Kim, Y. H., Min, S. K., Son, S. W., & Choi, J. (2017). Attribution of the local Hadley cell widening in the Southern Hemisphere. *Geophysical Research Letters*, *44*, 1015–1024. https://doi.org/10.1002/2016GL072353
Large, W., & Yeager, S. (2009). The global climatology of an interannually varying air-sea flux data set. *Climate dynamics*, *33*(2-3), 341–364.
Lesieur, M., Garnier, E., & Metais, O. (2000). Baroclinic instability and severe storms. Taylor & Francis.
Lu, J., Chen, G., & Frierson, D. M. (2008). Response of the zonal mean atmospheric circulation to El Niño versus global warming. *Journal of Climate*, *21*(22), 5835–5851.
Lu, J., Vecchi, G. A., & Reichler, T. (2007). Expansion of the Hadley cell under global warming. *Geophysical Research Letters*, *34*, L06805. https://doi.org/10.1029/2006GL028443
Lucas, C., & Nguyen, H. (2015). Regional characteristics of tropical expansion and the role of climate variability. *Journal of Geophysical Research: Atmospheres*, *120*, 6809–6824. https://doi.org/10.1002/2015JD023130
Mantsis, D. F., Sherwood, S., Allen, R., & Shi, L. (2017). Natural variations of tropical width and recent trends. *Geophysical Research Letters*, *44*, 3825–3832. https://doi.org/10.1002/2016gl072097
Mantua, N. J., Hare, S. R., Zhang, Y., Wallace, J. M., & Francis, R. C. (1997). A Pacific interdecadal climate oscillation with impacts on salmon production. *Bulletin of the american Meteorological Society*, *78*(6), 1069–1080.
Medeiros, B., Stevens, B., & Bony, S. (2015). Using aquaplanets to understand the robust responses of comprehensive climate models to forcing. *Climate Dynamics*, *44*(7-8), 1957–1977.
Nakamura, H., Sampe, T., Tanimoto, Y., & Shimpo, A. (2004). Observed associations among storm tracks, jet streams and midlatitude oceanic fronts. *Earths Climate: The Ocean–Atmosphere Interaction, Geophysical Monograph*, *147*, 329–345.
Nguyen, H., Evans, A., Lucas, C., Smith, I., & Timbal, B. (2013). The Hadley circulation in reanalyses: Climatology, variability, and change. *Journal of Climate*, *26*(10), 3357–3376.
Norris, J. R., Allen, R. J., Evan, A. T., Zelinka, M. D., OíDell, C. W., & Klein, S. A. (2016). Evidence for climate change in the satellite cloud record. *Nature*, *536*(7614), 72–75.
Orr, A., Bracegirdle, T. J., Hosking, J. S., Feng, W., Roscoe, H. K., & Haigh, J. D. (2012). Strong dynamical modulation of the cooling of the polar stratosphere associated with the Antarctic ozone hole. *Journal of Climate*, *26*(2), 662–668.
Petit, J. R., Jouzel, J., Raynaud, D., Barkov, N. I., Barnola, J. M., Basile, I., et al. (1999). Climate and atmospheric history of the past 420,000 years from the Vostok ice core, Antarctica. *Nature*, *399*(6735), 429.
Polvani, L. M., Waugh, D. W., Correa, G. J., & Son, S. W. (2011). Stratospheric ozone depletion: The main driver of twentieth-century atmospheric circulation changes in the Southern Hemisphere. *Journal of Climate*, *24*(3), 795–812.

Randel, W. J., & Wu, F. (1999). Cooling of the Arctic and Antarctic polar stratospheres due to ozone depletion. *Journal of Climate*, *12*(5), 1467–1479.

Rayner, N., Parker, D., Horton, E., Folland, C., Alexander, L., Rowell, D., & Kaplan, A. (2003). Global analyses of sea surface temperature, sea ice, and night marine air temperature since the late nineteenth century. *Journal of Geophysical Research*, *108*(D14), 4407. https://doi.org/10.1029/2002JD002670

Sampe, T., Nakamura, H., Goto, A., & Ohfuchi, W. (2010). Significance of a midlatitude SST frontal zone in the formation of a storm track and an eddy-driven westerly jet. *Journal of Climate*, *23*(7), 1793–1814.

Scheff, J., & Frierson, D. (2012). Twenty-first-century multimodel subtropical precipitation declines are mostly midlatitude shifts. *Journal of Climate*, *25*(12), 4330–4347.

Seidel, D. J., Fu, Q., Randel, W. J., & Reichler, T. J. (2008). Widening of the tropical belt in a changing climate. *Nature Geoscience*, *1*(1), 21–24.

Shaw, T. A. (2019). Mechanisms of future predicted changes in the zonal mean mid-latitude circulation. *Current Climate Change Reports*, *5*(4), 345–357.

Shaw, T. A., & Tan, Z. (2018). Testing latitudinally dependent explanations of the circulation response to increased $CO_2$ using aquaplanet models. *Geophysical Research Letters*, *45*, 9861–9869. https://doi.org/10.1029/2018GL078974

Son, S. W., Kim, S. Y., & Min, S. K. (2018). Widening of the Hadley cell from Last Glacial Maximum to future climate. *Journal of Climate*, *31*(1), 267–281.

Staten, P. W., Grise, K. M., Davis, S. M., Karnauskas, K., & Davis, N. (2019). Regional widening of tropical overturning: Forced change, natural variability, and recent trends. *Journal of Geophysical Research: Atmospheres*, *124*, 6104–6119. https://doi.org/10.1029/2018JD030100

Staten, P. W., Lu, J., Grise, K. M., Davis, S. M., & Birner, T. (2018). Re-examining tropical expansion. *Nature Climate Change*, *8*, 768–775.

Staten, P. W., Reichler, T., & Lu, J. (2014). The transient circulation response to radiative forcings and sea surface warming. *Journal of Climate*, *27*(24), 9323–9336.

Staten, P. W., Rutz, J. J., Reichler, T., & Lu, J. (2012). Breaking down the tropospheric circulation response by forcing. *Climate dynamics*, *39*(9-10), 2361–2375.

Tandon, N. F., & Cane, M. A. (2017). Which way will the circulation shift in a changing climate? Possible nonlinearity of extratropical cloud feedbacks. *Climate Dynamics*, *48*(11-12), 3759–3777.

Tandon, N. F., Gerber, E. P., Sobel, A. H., & Polvani, L. M. (2013). Understanding Hadley cell expansion versus contraction: Insights from simplified models and implications for recent observations. *Journal of climate*, *26*(12), 4304–4321.

Taylor, K. E., Stouffer, R. J., & Meehl, G. A. (2012). An overview of CMIP5 and the experiment design. *Bulletin of the American Meteorological Society*, *93*(4), 485–498.

Thompson, D. W., Solomon, S., Kushner, P. J., England, M. H., Grise, K. M., & Karoly, D. J. (2011). Signatures of the Antarctic ozone hole in Southern Hemisphere surface climate change. *Nature Geoscience*, *4*(11), 741.

Toggweiler, J. R., & Russell, J. (2008). Ocean circulation in a warming climate. *Nature*, *451*(7176), 286.

Wang, Q., Danilov, S., Sidorenko, D., Timmermann, R., Wekerle, C., Wang, X., & Schröter, J. (2014). The Finite Element Sea Ice-Ocean Model (FESOM) v. 1.4: Formulation of an ocean general circulation model. *Geoscientific Model Development*, *7*(2), 663–693.

Waugh, D. W., Grise, K. M., Seviour, W. J., Davis, S. M., Davis, N., Adam, O., et al. (2018). Revisiting the relationship among metrics of tropical expansion. *Journal of Climate*, *31*(18), 7565–7581.

Yang, H., Lohmann, G., Krebs-Kanzow, U., Ionita, M., Shi, X., Sidorenko, D., & Gowan, E. J. (2020). Poleward shift of the major ocean gyres detected in a warming climate. *Geophysical Research Letters*, *47*, e2019GL085868. https://doi.org/10.1029/2019GL085868

Yang, H., Lohmann, G., Shi, X., & Li, C. (2019). Enhanced mid-latitude meridional heat imbalance induced by the ocean. *Atmosphere*, *10*(12), 746.

Yang, H., Lohmann, G., Wei, W., Dima, M., Ionita, M., & Liu, J. (2016). Intensification and poleward shift of subtropical western boundary currents in a warming climate. *Journal of Geophysical Research: Oceans*, *121*, 4928–4945. https://doi.org/10.1002/2015JC011513

Yin, J. H. (2005). A consistent poleward shift of the storm tracks in simulations of 21st century climate. *Geophysical Research Letters*, *32*, L18701. https://doi.org/10.1029/2005GL023684

Zhou, C., Lu, J., Hu, Y., & Zelinka, M. D. (2020). Responses of the Hadley circulation to regional sea surface temperature changes. *Journal of Climate*, *33*(2), 429–441.